01

Method for determining the configuration of a protective film at numerical simulation of pulsation modes of convective-film coolings

© A.L. Tukmakov, A.A. Akhunov, N.A. Tukmakova, V.V. Kharkov

Kazan National Research Technical University named after A. N. Tupolev KAI,
Kazan , Russia
e-mail: tukmakov@imm.knc.ru

Received February 15, 2023
Revised April 10, 2023
Accepted April 11, 2023

Presented is a method of determining the configuration of a protective film during numerical modeling of systems convective-film cooling on the example of double-sided flow around the plate with high-temperature and cooling flows communicating through an inclined slit channel that connects the regions cooling and high-temperature gas flow. Gas dynamic field calculations were performed for both of the plate side, and the configuration of the cooling film in the pulsating supply of the cooling film is described air.

Keywords: numerical modeling, Navier–Stokes equations, Mac–Cormac scheme, multi-connected regions, wall functions, convective-film cooling.

DOI: 10.61011/TP.2023.06.56523.26-23

Introduction

Convective-film cooling systems are used to protect nozzle and moving blading of turbines operating in high-temperature gas flows [1]. The efficiency of film cooling depends both on the shape of the channels connecting the flow area of the cooling and high-temperature flows, and on the coolant feed mode — stationary or pulsating. In order to increase the cooling efficiency the various types of channels were developed: cylindrical, reradiating, radial, cantilever, conical, reradiating-radial, anti-vortex, pair, louvre, etc. [2]. The cooling efficiency depends on the configuration of the protective film created by the cooling jets near the surface to be protected. The study of such systems and the search for the best form of channels both in stationary and pulsating modes are often carried out by methods of mathematical modeling. In this case, it is desirable to know what the shape of the protective film will be for a particular flow mode and the profile of the channel through which the cooling gas is fed. The shape of the film can be estimated from the thermal field configuration in the vicinity of the outlet section of the channel, but in this case the result is integral and is determined by the interaction of the high-temperature and cooling flows. At the same time, the shape of the cold gas jet injected into the main flow is interesting, the jet creates a curtain [3–6] and can change in pulsating modes [7,8]. In the present paper it is proposed to estimate the film configuration not only on the basis of the temperature field, but also on the basis of the spatial distribution of the cold component of the gaseous mixture blown into the hot flow region. In this case, the calculation can be carried out on the basis of a dynamics model of the two-component gas, and the film shape can be compared with the density distribution of the low-temperature component in the hot flow region.

1. Equations of gas motion, statement of the problem and method of its solution

To describe the non-stationary process of the protective film formation, a system of equations of motion of a viscous compressible heat-conducting two-component gas was used, which was written in generalized curvilinear coordinates $\xi = \xi(x, y)$, $\eta = \eta(x, y)$, where (x, y) — physical, and ξ, η — calculated coordinates [9–11]. The system of equations and the method for solving it are described in the Appendix.

The protective film is formed when the cooling gas jet interacts with the high-temperature stream. Fig. 1 shows the results of the verification calculation of the flow of the flat submerged air jet in the stationary mode. The computational domain is shown in Fig. 1, *a*. The jet parameters are set using boundary conditions. At $y = 0$, $0 < x < 0.48$ m, $0.52\,\text{m} < x < 1\,\text{m}$ the no-slip conditions are set for the gas velocity. At $y = 0$, $0.48\,\text{m} < x < 0.52\,\text{m}$ the gas velocity is set: $u = 0$, $v = 4$ m/s, where u, v — gas velocity components in the direction of axes $0x$, $0y$. On the other boundaries of the computational domain for the velocity components the uniform Neumann conditions are set. Neumann conditions are also set for the density, pressure, and energy at all boundaries of the computational domain. At the initial time, the gas is stationary, its temperature $T = 400$ K, component densities $\rho_1 = \rho_2 = 0.645\,\text{kg/m}^3$ are set. Fig. 1, *a* shows the jet shape and the velocity distribution in the jet in the stationary mode. Fig. 1, *b* shows the stationary values of the vertical velocity component at various points on the jet axis: *1* — $y = 0.005$ m, *2* — $y = 0.25$ m, *3* — $y = 0.5$ m, *4* — $y \approx 1$ m. The cross sections of the jet plotted with the step $\Delta y = 0.128$ m are

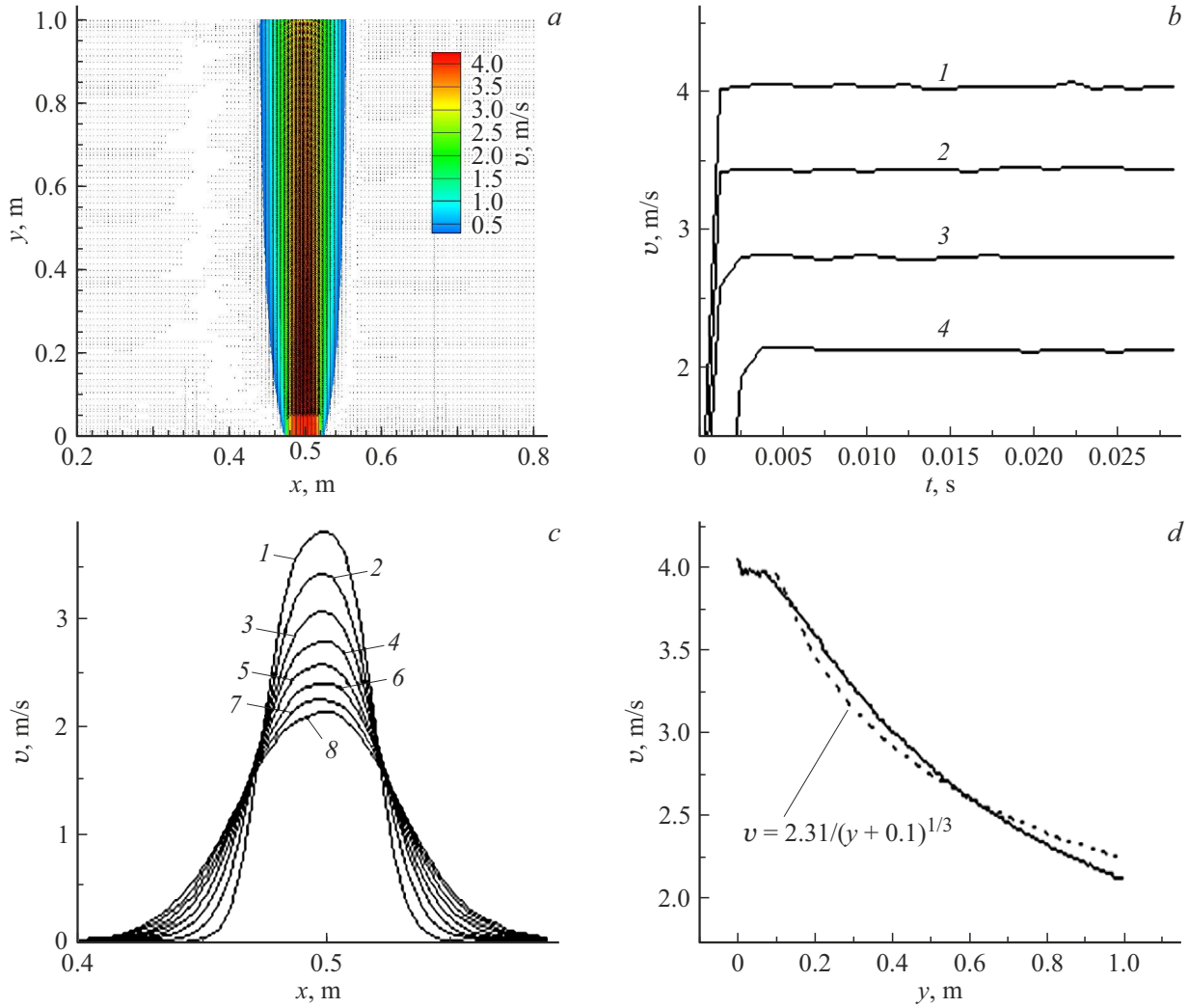

Figure 1. Flat submerged jet: *a* — jet velocity field, *b* — velocity settling process, *c* — velocity profiles in jet cross sections, *d* — longitudinal velocity distribution on the jet axis.

shown in Fig. 1, *c*: the curve *1* was plotted at $y = 0.1$ m, curve *8* — at $y = 1$ m. The velocity distribution along the jet axis is shown in Fig. 1, *d* by the solid line. The dashed line — approximation by function $v \approx 2.31/(y + 0.1)^{1/3}$ at $y > 0$. The jet center is at $x = 0.5$ m, $y \approx -0.1$ m. The exponent 1/3 in the denominator of the obtained approximating dependence corresponds to the laminar flow mode of the flat jet [12,13].

The technique that makes it possible to determine the configuration of the protective film from the density distribution of the cooling gas is described below using the example of solving the problem of convective-film cooling of the plate with a slotted channel. Fig. 2 shows a diagram of the computational domain, which includes the plate with an inclined slotted channel.

The plate $h = 0.003$ m thick separates the flows of low-temperature (region I) and hot gas (region V). Computational domain length is $L = 0.16$ m, heights are $h_1 = 0.1$ m, $h_2 = 0.08$ m (Fig. 2, *a*). Distance along the plate from the inlet section to the side wall of the inclined slot is $\ell = 0.07$ m. Fig. 2, *b* shows the fragment of the computational domain of a block-structured finite difference grid constructed by the Thompson method [10].

Since the protective film configuration is determined by the cold component distribution, it is proposed to use in flow calculations a single-velocity two-component model of the motion of the viscous compressible heat-conducting gas. This model comprises two gas components — high temperature with density ρ_1 and cooling with density ρ_2. The system of equations includes a continuity equation for each component, as well as conservation equations for pulse components and energy conservation equation for the mixture as a whole. Thus, two continuity equations are used to calculate the gas density:

$$\partial\rho_1/\partial t + \partial(\rho_1 u)/\partial x + \partial(\rho_1 v)\partial y = div(v_1 \nabla\rho_1),$$

$$\partial\rho_2/\partial t + \partial(\rho_2 u)/\partial x + \partial(\rho_2 v)\partial y = div(v_1 \nabla\rho_2),$$

$$\rho = \rho_1 + \rho_2.$$

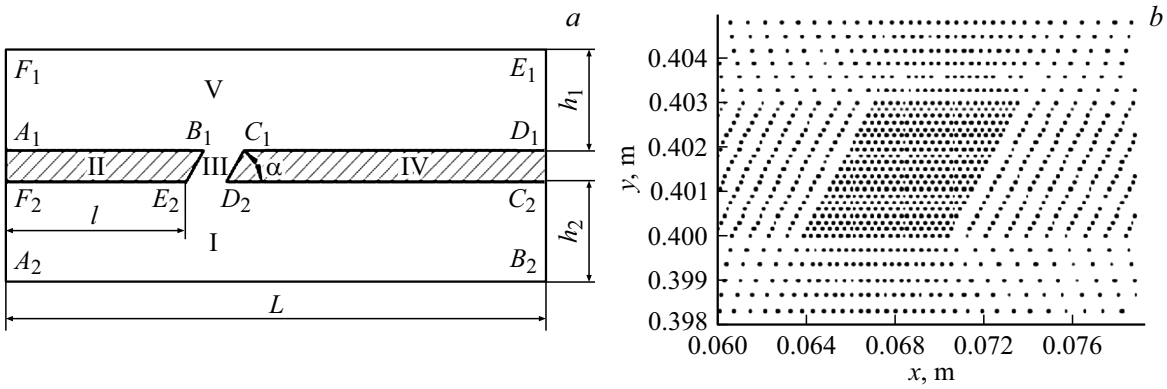

Figure 2. *a* — scheme of the computational domain, *b* — fragment of the finite-difference grid in the vicinity of the channel.

Therefore, air in high-temperature and low-temperature streams consists of two „components“ with the same properties, velocities and temperatures at each node of the finite-difference grid, but differently distributed in the low-temperature and high-temperature parts of the computational domain. Let at the initial moment of time the densities of the components be distributed as follows: — in region V: $\rho_1 = \rho_{10} - \alpha_{20}$, $\rho_2 = \alpha_{20}$, $\rho = \rho_1 + \rho_2 = \alpha_{10}$ at $\alpha_{20} \ll \rho_{10}$; in region I: $\rho_2 = \rho_{20} - \alpha_{10}$, $\rho_1 = \alpha_{10}$, $\rho = \rho_1 + \rho_2 = \alpha_{20}$ at $\alpha_{10} \ll \rho_{20}$.

Thus, the gas in region I consists of component 2 with a small addition of component 1, while they have the same physical properties, temperature, and velocity components. In region V before mixing with the cooling jet the gas consists of component 1 with a small addition of component 2. In this case, the physical properties, temperatures and velocities of the first and second components in each node are the same. The total air density is equal to the sum of the component densities: $\rho = \rho_1 + \rho_2$. Further, the total density is used in the conservation equations of pulse components and in the energy conservation equation.

Since the carrier of the low gas temperature in the region V is the second component of the mixture, its distribution in the region V determines the protective film configuration. The carrier of high temperature in region I is the first component of the mixture. Its presence in region I indicates the hot air inflow into the region of the cooling stream, which is possible when the coolant is supplied in pulsating modes.

Let at the initial moment of time the temperatures and densities of the stationary gas at the nodes of the gas-dynamic grid are: $T_{20} = 400\,\mathrm{K}$, $\rho_{20} = 1.2\,\mathrm{kg/m^3}$, $T_{10} = 600\,\mathrm{K}$, $\rho_{10} = 0.58\,\mathrm{kg/m^3}$, and temperature at the nodes of the solid grid is $T = T_{20}$. Gas pressure at inlet and outlet of the region I was: $p_+ = (1.1 + 0.3\sin(2\pi f \times t))p_{20}$, $p_- = 0.9p_{20}$, where $p_{20} = 128\,\mathrm{kPa}$ — initial gas pressure in the region I (Fig. 2, *a*), f — linear frequency of oscillations. In region V $p_+ = 1.1p_{10}$, $p_- = 0.9p_{10}$, where $p_{10} = 120.5\,\mathrm{kPa}$ — initial gas pressure in the region V.

Further calculations are made using grids with number of nodes $N_j \times N_k = 200 \times 200$. In this case, the near-wall grid nodes closest to the plate surface on both sides of the plate were located at the beginning of the logarithmic regions of the velocity boundary layers at $30 \le y^+ \le 60$.

2. Calculation results

As an example, Fig. 3 shows the process of temperature establishing at the point $(x = L/2,\ y = h_2 + h + h_{1/2})$, located on the longitudinal axis of the high-temperature region V, above the outlet section of the slotted channel for the oscillation frequency of gas pressure in the cooling channel $f = 500\,\mathrm{Hz}$ and at the amplitude of pressure oscillations $0.3p_{20}$.

The oscillations are non-linear, have asymmetric leading and trailing edges. Comparison of time dependences for velocity with dependences for temperature, density, pressure shows that the velocity oscillations in phase are ahead of temperature, density and pressure oscillations by approximately $T/4$, where $T = 0.002\,\mathrm{s}$ — oscillation period. Fig. 4 shows the distribution of gas temperature in the near-wall layer of nodes along the upper surface

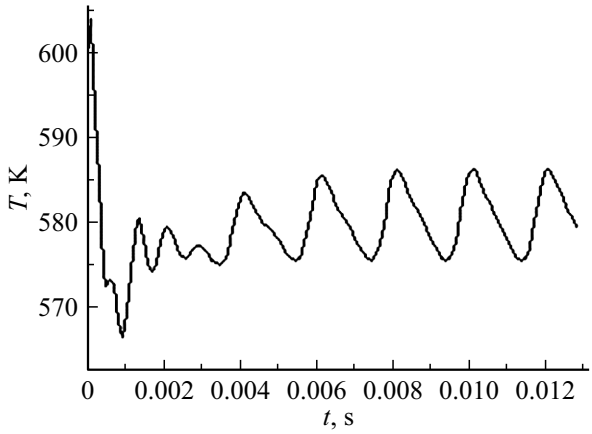

Figure 3. Time dependence of temperature at the point $(x = L/2,\ y = h_2 + h + h_1/2)$ at oscillation frequency $f = 500\,\mathrm{Hz}$.

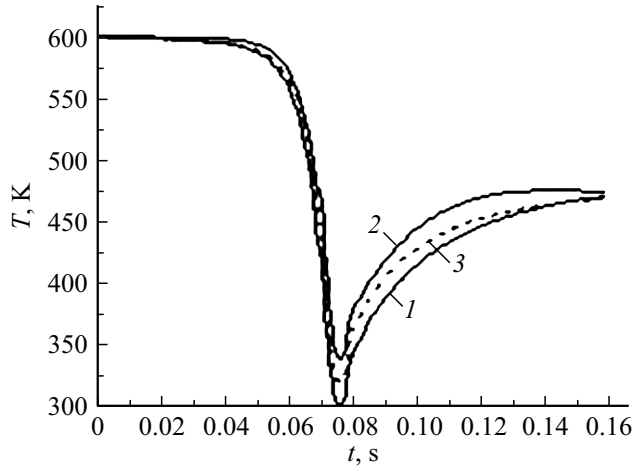

Figure 4. Gas temperature distribution near the outer surface of the plate at times, t: *1* — 0.0052, *2* — 0.0057 s, *3* — stationary temperature distribution.

of the plate (Fig. 2, *a*) at time moments $t_1 = 0.0052$ s, $t_2 = 0.0057$ s spaced by $T/4$ during the oscillation period. The minimum temperature is reached at the outlet section of the slotted channel. Upstream of the outlet section, during the oscillation period, the temperature along the surface rises faster than downstream, where the protective film is formed. In this case, the temperature difference in the region located below the outlet section of the slot and lying at the base of the protective film adjacent to the surface, during the oscillation period reaches $\Delta T = 40$ K (Fig. 4).

Fig. 5, *a, c* shows the spatial density distribution of the second (cold) component ρ_2 in the high-temperature region at times $t = 0.0052$ and 0.0057 s. Fig. 5, *b, d* shows the spatial distribution of the gas temperature at the same time moments. Both parameters allow you to evaluate the location of the protective film.

Calculations show that at $t = 0.0052$ s, the film occupies a larger volume (Fig. 5, *a*) and has a greater extent of the cold core along the plate from the blowing in point (Fig. 5, *b*). After a quarter of the period, at $t = 0.0057$ s, the volume of the film (Fig. 5, *c*) and its cold core (Fig. 5, *d*) decreases, the film is pressed against the surface to be protected.

Calculations show that in the upward direction relative to the high-temperature flow, the effect of non-stationarity of the cooling jet on the film shape manifests itself

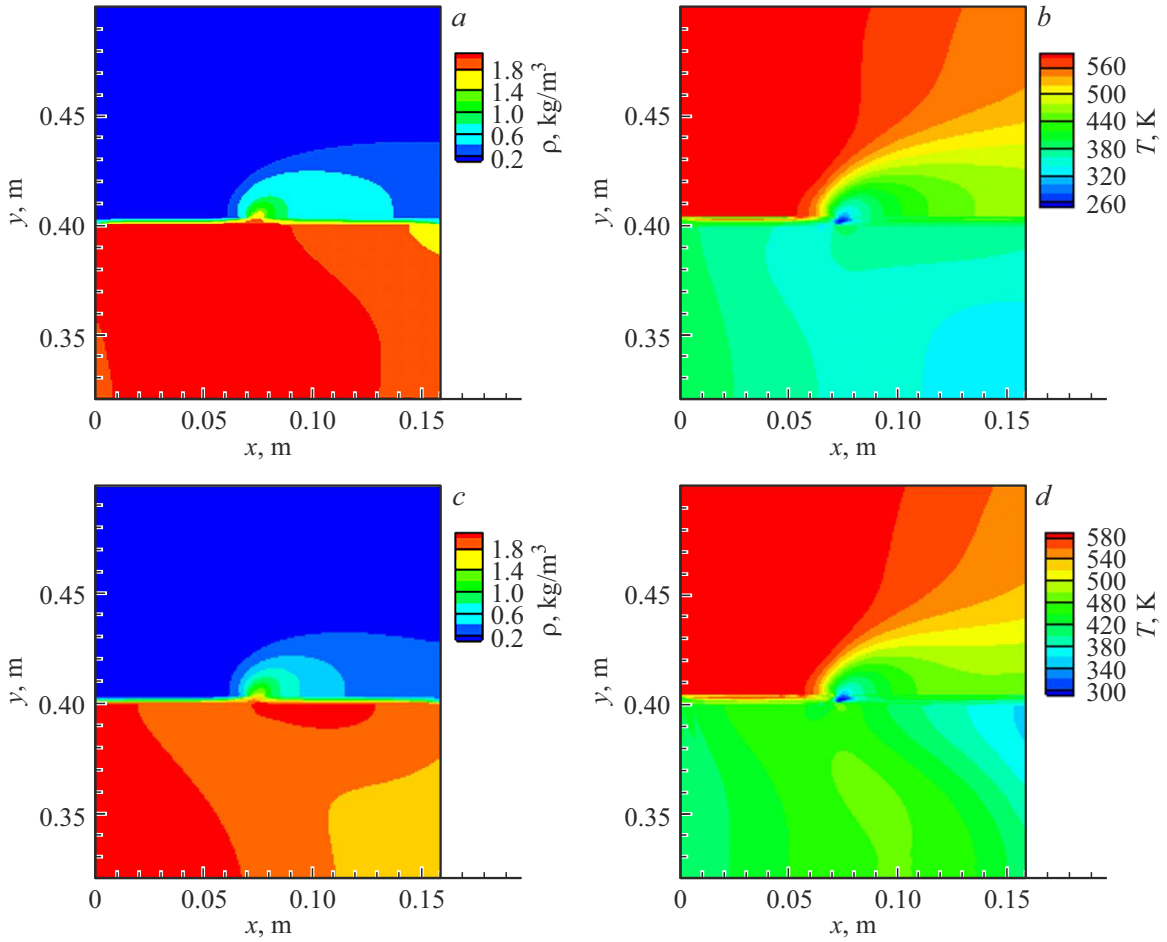

Figure 5. The shape of the protective film at different times: *a* — density of the cold component ρ_2; *b* — gas temperature at time $t = 0.0052$ s; *c* — cold component density ρ_2; *d* — gas temperature at time $t = 0.0057$ s.

insignificantly, while in the direction of the flow, during the oscillation period, the film dimensions change significantly. If at time $t = 0.0052$ s the right boundary of the protective film, on which the density of the second component reaches the value $\rho_2 = 0.6$ kg/m ^{3}, is located at $x \approx 0.135$ m (Fig. 5, *a*), then at time $t = 0.0057$ s the protective film approaches the plate, and its right boundary, at which the density is $\rho_2 = 0.6$ kg/m ^{3}, is at $x \approx 0.11$ m (Fig. 5, *c*).

Conclusion

The shape of the protective film and its location relative to the surface determine the cooling efficiency and depend on the parameters of the high-temperature gas flow, the method of feeding the cooling gas, and the shape of the channel in which the jet is formed. In numerical simulation using single-velocity two-component gas flow model, the film shape can be determined from the distribution of the main gas component for the cooling stream in the high-temperature flow. This method of determining the film configuration complements the estimate obtained from the construction of the temperature field.

Funding

This study was supported by the Russian Science Foundation, project № 22-19-00207, https://rscf.ru/project/22-19-00207/.

Conflict of interest

The authors declare that they have no conflict of interest.

Appendix

System of equations of motion of viscous compressible heat-conducting two-component gas and method of its solution

The system of equations of motion of viscous compressible heat-conducting gas in generalized curvilinear coordinates has the form [9,10]:

$$\mathbf{q}_t + \mathbf{F}_\xi + \mathbf{G}_\eta = \mathbf{H} \qquad (\Pi 1)$$

$$\mathbf{q} = \left[\frac{\rho_1}{J}, \frac{\rho_2}{J}, \frac{\rho u}{J}, \frac{\rho v}{J}, \frac{E}{J}\right]^T,$$

$$\mathbf{F} = \frac{1}{J}\begin{bmatrix} \xi_x\rho_1 u + \xi_y\rho_1 v \\ \xi_x\rho_2 u + \xi_y\rho_2 v \\ \xi_x(\rho u^2 + p - \tau_{xx}) + \xi_y(\rho uv - \tau_{xy}) \\ \xi_x(\rho uv - \tau_{xy}) + \xi_y(\rho v^2 + p - \tau_{yy}) \\ \xi_x\big((E + p - \tau_{xx})u - \tau_{xy}v + Q_x\big) \\ +\xi_y\big((E + p - \tau_{yy})v - \tau_{xy}u + Q_y\big) \end{bmatrix},$$

$$\mathbf{G} = \frac{1}{J}\begin{bmatrix} \eta_x\rho_1 u + \eta_y\rho_1 v \\ \eta_x\rho_2 u + \eta_y\rho_2 v \\ \eta_x(\rho u^2 + p - \tau_{xx}) + \eta_y(\rho uv - \tau_{xy}) \\ \eta_x(\rho uv - \tau_{xy}) + \eta_y(\rho v^2 + p - \tau_{yy}) \\ \eta_x\big((E + p - \tau_{xx})u - \tau_{xy}v + Q_x\big) \\ +\eta_y\big((E + p - \tau_{yy})v - \tau_{xy}u + Q_y\big) \end{bmatrix},$$

$$\mathbf{H} = \frac{1}{J}\begin{bmatrix} div(v_t\nabla\rho_1) \\ div(v_t\nabla\rho_2) \\ 0 \\ 0 \\ 0 \end{bmatrix}, \qquad \rho = \rho_1 + \rho_2,$$

$$\tau_{yx} = \tau_{xy}; \quad \tau_{xy} = (\mu + \mu_t)\left(\frac{\partial u}{\partial y} + \frac{\partial v}{\partial x}\right),$$

$$\tau_{xx} = 2(\mu + \mu_t)\frac{\partial u}{\partial x} - \frac{2}{3}(\mu + \mu_t)div(U),$$

$$\tau_{yy} = 2(\mu + \mu_t)\frac{\partial v}{\partial y} - \frac{2}{3}(\mu + \mu_t)\cdot div(U),$$

$$p = (\gamma - 1)\rho I, \qquad E = I + 0.5\rho(u^2 + v^2),$$

$$Q_x = -(\mathbf{k} + C_p\mu_t/\mathrm{Pr})\partial t/\partial x,$$

$$Q_y = -(\mathbf{k} + C_p\mu_t/\mathrm{Pr})\partial T/\partial y,$$

$$div(U) = \partial u/\partial x + \partial v/\partial y.$$

Here ρ, ρ_1, ρ_2, u, v, E, I, T, p — density of gas and components, longitudinal and transverse velocity components, total and internal energy , temperature and gas pressure; γ, μ, μ_t — adiabatic constant, dynamic molecular and turbulent gas viscosities; Pr — Prandtl number; τ_{xx}, τ_{yy}, τ_{xy} — viscous stress tensor components. The internal energy of the gas was defined as $I = \rho C_V T$, where C_V — specific heat at constant volume, and the gas temperature is $T = \big(E - 0.5\rho(u^2 + v^2)\big)/\rho C_V$. When writing the continuity equations for the components, the concentration diffusion of the gas is taken into account. The metric coefficients and the Jacobian of the transition from calculated to physical coordinates are defined as [9,10]: $\xi_x = J \cdot y_\eta$, $\xi_y = -J \cdot x_\eta$, $\eta_x = -J \cdot y_\xi$, $\eta_y = J \cdot x_\xi$, $J = \xi_x\eta_y - \xi_y\eta_x$.

System (A1) was solved by the explicit second-order McCormack method [9,10] with splitting of the original operator in spatial directions [9,11]:

$$q^{n+1}_{j,k} = P_\xi(\Delta t_\xi/2)P_\eta(\Delta t_\eta/2)P_\eta(\Delta t_\eta/2)P_\xi(\Delta t_\xi/2)q^n_{j,k}. \qquad (\Pi 2)$$

The transition from the time layer t^n to the layer t^{n+1} by applying one-dimensional operators to the vector of gas-dynamic functions from the previous layer is carried out as follows:

$$\mathbf{q}^{(1)}_{j,k} = \mathbf{P}_\xi(\Delta t_\xi/2)\mathbf{q}^n_{j,k}, \quad \mathbf{q}^{(2)}_{j,k} = \mathbf{P}_\eta(\Delta t_\eta/2)\mathbf{q}^{(1)}_{j,k},$$

$$\mathbf{q}_{j,k}^{(3)} = \mathbf{P}_\eta(\Delta t_\eta/2)\mathbf{q}_{j,k}^{(2)}, \quad \mathbf{q}_{j,k}^{(n+1)} = \mathbf{P}_\xi(\Delta t_\xi/2)\mathbf{q}_{j,k}^{(3)}. \qquad (\Pi 3)$$

Here $\Delta t_\xi = \Delta t_\eta = \Delta t$. So, to obtain intermediate values of the vector $\mathbf{q}^{(1)}$, it is necessary to apply the one-dimensional operator $\mathbf{P}_\xi(\Delta t_x/2)$ on the variable ξ to the vector of gas-dynamic functions on the time layer t^n. The action of each one-dimensional operator $\mathbf{P}$ consists in successive execution of the steps „predictor“ and „corrector“ on the corresponding spatial variable:

$$\mathbf{q}_{j,k}^{(1)^*} = \mathbf{q}_{j,k}^n - \frac{(\Delta t_\xi/2)}{\Delta\xi}\left(\mathbf{F}_{j+1,k}^n - \mathbf{F}_{j,k}^n\right), \qquad (\Pi 4)$$

$$\mathbf{q}_{j,k}^{(1)} = 0.5\left(\mathbf{q}_{j,k}^n + \mathbf{q}_{j,k}^{(1)^*}\right) - 0.5\frac{(\Delta t_\xi/2)}{\Delta\xi}\left(\mathbf{F}_{j,k}^{(1)^*} - \mathbf{F}_{j-1.k}^{(1)^*}\right), \qquad (\Pi 5)$$

$$\mathbf{q}_{j,k}^{(2)^*} = \mathbf{q}_{j,k}^1 - \frac{\Delta t_\eta/2}{\Delta\eta}\left(\mathbf{G}_{j,k+1}^{(1)} - \mathbf{G}_{j,k}^{(1)}\right), \qquad (\Pi 6)$$

$$\mathbf{q}_{\mathbf{j,k}}^{(\mathbf{2})} = 0.5\left(\mathbf{q}_{j,k}^1 + \mathbf{q}_{j,k}^{(2)^*}\right) - 0.5\frac{(\Delta t_\eta/2)}{\Delta\eta}\left(\mathbf{G}_{j,k}^{(2)^*} - \mathbf{G}_{j,k-1}^{(2)^*}\right), \qquad (\Pi 7)$$

etc. At the step „predictor“ the approximation of the derivatives in ξ, included in $\mathbf{F}_{j+1,k}^n$, $\mathbf{F}_{j,k}^n$, is performed using the left difference scheme of the first order of accuracy, at the step „corrector“ — with the help of the right one, and the derivatives in η are approximated by second-order central difference schemes. Derivatives in η, included in $\mathbf{G}_{j,k+1}^n$, $\mathbf{G}_{j,k}^n$, are approximated at the step „predictor“ step by left first-order difference schemes, and at the step „corrector“ by the right schemes. Difference derivatives in ξ in $\mathbf{G}_{j,k+1}^n$, $\mathbf{G}_{j,k}^n$ at each step are central.

To describe the transfer of the modified kinematic turbulent viscosity ν, the basic Spalart–Allmaras model is used [14,15]:

$$\frac{\partial(\nu)}{\partial t} + \frac{\partial(u\nu)}{\partial x} + \frac{\partial\nu\nu}{\partial y} = \frac{\partial}{\partial x}\left(\frac{\nu_0+\nu}{\sigma_\nu}\frac{\nu}{\partial x}\right) + \frac{\partial}{\partial y}\left(\frac{\nu_0+\nu}{\sigma_\nu}\frac{\partial\nu}{\partial y}\right) + \frac{C_{b2}}{\sigma_\nu}\left(\left(\frac{\partial\nu}{\partial x}\right)^2 + \left(\frac{\partial\nu}{\partial y}\right)^2\right) + P_\nu - \varepsilon_\nu. \qquad (\Pi 8)$$

Here P_ν, ε_ν, ν_0, ν — the rate of generation and dissipation of turbulent viscosity, molecular and modified kinematic viscosity. When using the Spalart-Allmaras model, the parameter k^{te} is omitted in the expressions for Reynolds stresses. The kinematic turbulent viscosity ν_t is determined through the modified kinematic turbulent viscosity ν:

$$\nu_t = \nu \times F_{\nu 1}, \quad f_{\nu 1} = \frac{\Lambda^3}{\Lambda^3 + C_{\nu 1}^3}, \quad \Lambda = \frac{\nu}{\nu_0},$$

$$P_\nu = C_{b1}S\nu, \quad S = |\Omega| + \frac{\nu}{(kd)^2}f_{\nu 2},$$

$$f_{\nu 2} = 1 - \frac{\Lambda}{1+\Lambda f_{\nu 1}}, \quad \varepsilon_\nu = C_{w1}f_w\left(\frac{\nu}{d}\right)^2,$$

$$f_w = g\left(\frac{1+C_{w3}^6}{g^6+C_{w3}^6}\right)^{1/6}, \quad C_{w1} = \frac{C_{b1}}{k^2} + \frac{1+C_{b2}}{\sigma_\nu},$$

$$g = r + C_{w2}(r^6 - r), \quad r = \frac{\nu}{(kd)^2 S}.$$

Here d — the closest distance to the wall, $k = 0.4187$ — Karman constant. The vorticity modulus Ω is defined as

$$\Omega = \frac{1}{\sqrt{2}}\left|\frac{\partial u}{\partial y} - \frac{\partial\nu}{\partial x}\right|.$$

Values of the base model constants:

$$C_{b1} = 0.1355, \quad C_{b2} = 0.622, \quad \sigma_\nu = 2/3,$$

$$C_{\nu 1} = 7.1, \quad C_{w2} = 0.3, \quad C_{w3} = 2.$$

Kinematic turbulent viscosity is related to dynamic turbulent viscosity by the relation $\mu_t = \rho\nu_t$. Spalart–Allmaras equation was written in generalized curvilinear coordinates in a quasi-conservative form (P9) and solved

$$\frac{\partial\nu_1}{\partial t} + \frac{\partial F}{\partial\xi} + \frac{\partial G}{\partial\eta} = H, \qquad (\Pi 9)$$

$$\nu_1 = \frac{\nu}{J}, \quad F = \frac{\xi_t\nu + \xi_x u\nu + \xi_y\upsilon\nu}{J},$$

$$G = \frac{\eta_t\nu + \eta_x u\nu + \eta\upsilon\nu}{J},$$

$$H = \frac{\partial}{\partial x}\left(\frac{(\nu_0+\nu)}{\sigma_\nu}\frac{\partial\nu}{\partial x}\right) + \frac{\partial}{\partial y}\left(\frac{(\nu_0+\nu)}{\sigma_\nu}\frac{\partial\nu}{\partial y}\right) + \frac{C_{b2}}{\sigma y}\left(\left(\frac{\partial\nu}{\partial x}\right)^2 + \left(\frac{\partial\nu}{\partial y}\right)^2\right) + P_\nu - \varepsilon_\nu,$$

$$\frac{\partial\nu}{\partial x} = \nu_\xi\xi_x + \nu_\eta\eta_x, \qquad \frac{\partial\nu}{\partial y} = \nu_\xi\xi_y + \nu_\eta\eta_y,$$

$$\left(\frac{(\nu_0+\nu)}{\sigma_\nu}\frac{\partial\nu}{\partial x}\right)_x = \left(\frac{(\nu_0+\nu)}{\sigma_\nu}\frac{\partial\nu}{\partial x}\right)_\xi\xi_x + \left(\frac{(\nu_0+\nu)}{\sigma_\nu}\frac{\partial\nu}{\partial x}\right)_\eta\eta_x,$$

$$\left(\frac{(\nu_0+\nu)}{\sigma_\nu}\frac{\partial\nu}{\partial y}\right)_y = \left(\frac{(\nu_0+\nu)}{\sigma_\nu}\frac{\partial\nu}{\partial y}\right)_\xi\xi_y + \left(\frac{(\nu_0+\nu)}{\sigma_\nu}\frac{\partial\nu}{\partial y}\right)_\eta\eta_y$$

by McCormack explicit method with splitting of the spatial operator in directions and a nonlinear correction scheme, similar to how the equations of the system of motion of viscous compressible heat-conducting gas are solved.

The block-structured finite-difference grid was constructed by combining the grid blocks of the gas flow region shown in Fig. 2, *b*. Within each block, the Thompson method [10] was used to construct the grid. Grids of adjacent blocks, including solid ones, designed to solve

the problem of thermal conductivity, were built conformally with nodes coinciding at the boundaries of the blocks.

On the solid boundaries of the computational domain, the no-slip conditions were set for the velocity components, and for pressure, temperature, energy, and gas density — homogeneous boundary conditions of the second kind. At the inlet boundaries of the hot and cold gas flow regions pressure, density, and temperature were set, as well as homogeneous boundary conditions of the second kind for the velocity components. Pressure values were set at the outlet boundaries, and homogeneous boundary conditions of the second kind were set for the rest of the gas-dynamic functions. At the initial moment of time, the temperature, density, and gas velocity components were set in the internal nodes of the gas computational domain. At the nodes of the solid regions II, IV (Fig. 1) the plate temperature values were set.

To model the thermal boundary layer and determine the temperature of the plate surface, the velocity and thermal near-wall functions were used, which relate the dimensionless parameters $T^+ = (T_w - T_i)/T_\tau$ and $y^+ = \rho u_\tau d/\mu$. Here T_w — wall temperature at a given node on the plate surface; T_i — stream temperature in the gas-dynamic grid node nearest to it; $T_\tau = q_w/(\rho C_p u_\tau)$ — friction temperature [16]. The thermal near-wall function of the form [16] was used:

$$T^+(y^+) = \begin{cases} y^+\mathrm{Pr}, \ y^+\mathrm{Pr} < 1, \\ 1.87\ln(y^+\mathrm{Pr}+1) + 0.065y^+\mathrm{Pr} - 0.36, \\ \qquad 1 \le y^+\mathrm{Pr} \le 11.7 \\ 2.5\ln(y^+\mathrm{Pr}) - 1, \ y^+\mathrm{Pr} > 11.7) \end{cases}. \qquad (\Pi 10)$$

The values of the wall variables y^+ and $u^+ = u/u_\tau$, where $u_\tau = (\tau_w/\rho)^{1/2}$ — dynamic velocity, are found from the universal relation for Spaulding's self-modeling velocity profile [17] inside the viscous boundary layer:

$$\frac{\mathrm{Re}}{u^+} = u^+ + e^{-22}\left(e^{ku^+} - 1 - ku^+ - \frac{1}{2}(ku^+)^2 - \frac{1}{6}(ku^+)^3 - \frac{1}{24}(ku^+)^4\right), \qquad (\Pi 11)$$

where $k = 0.41$ — Karman constant, $\mathrm{Re} = \rho u d/\mu$ — known Reynolds number in the first wall node. With a known number Re at a given node, equation (P11) is solved iteratively by Newton's method with respect to the parameter u^+ at this node. Then $u_\tau = u/u^+$ and $y^+ = y u_\tau \rho/\mu$ are determined. When solving the system of equations of gas motion, the normal stress τ_{xx} in the near-wall nodes closest to the plate surface in the equations of conservation of the pulse components and energy is equal to the stress on the wall $\tau_w = \rho_\tau^2$, found using near-wall functions.

To assess the performance of the model, which includes the Spalart–Allmaras equation and the near-wall velocity functions the calculations of the turbulent gas flow around the flat plate were performed, and velocity profiles $u^+(\log(y^+))$ were plotted in sections located across the boundary layer. The dependences obtained in the logarithmic region of the boundary layer practically coincided with the Spolding self-modeling profile [17].

The heat flux is expressed in terms of the friction temperature and the parameter T^+ [16]: $q_w = (T_w - T_i)\rho C_p u_\tau/T^+$. Hence the heat transfer coefficient on the surface plate–gas is $\alpha = \rho C_p \mu_\tau/T^+$. Knowing the gas temperatures T_1, T_2 near the hot and cold surfaces of the plate in the nodes of the gas grid closest to the surface, the heat transfer coefficients of the surfaces α_1, α_2, the thermal conductivity of the plate λ and its thickness h, we find the temperatures at the nodes on the plate surfaces [18]:

$$T_{w,1} = T_1 - (k_c/\alpha_1)(T_1 - T_2),$$

$$T_{w,2} = T_2 - (k_c/\alpha_2)(T_1 - T_2), \qquad (\Pi 12)$$

where $\alpha_1 = \rho_1 C_p u_{\tau 1}/T_1^*$, $\alpha_2 = \rho_2 C_p u_{\tau 2}/T_2^*$ — heat transfer coefficients from side of hot and cold streams; $k_c = (1/\alpha_1 + 1/\alpha_2 + h/\lambda)^{-1}$ — wall heat transfer coefficient.

References

[1] A.V. Shchukin, A.V. Il'inkov, V.V. Takmovtsev, T.A. Il'inkova, I.I. Khabibullin. *Teplofizika rabochikh protsesov v okhlazhdaemykh lopatkakh gazovykh turbin* (KNITU-KAI, Kazan, 2020) (in Russian)

[2] S. Acharya, Y. Kanani. *Advances in Film Cooling Heat Transfer. In book: Advances in Heat Transfer*, 49, 91–156 (Elsevier, 2017), DOI: 10.1016/bs.aint.2017.10.001

[3] S.V. Ekkad, S. Ou, R.B. Rivir. J. Turbomach, **128** (3), 564 (2006).

[4] S. Ou, R.B. Rivir. *Shaped-Hole Film Cooling With Pulsed Secondary Flow, Volume 3: Heat Transfer, Parts A and B* (ASMEDC, 2006), p. 259–269.

[5] L.A. El-Gabry, R.B. Rivir. J. Turbomach, **134** (4), 041005 (2012).

[6] J.L. Rutledge, P.I. King, R.B. Rivir. *CFD Predictions of Pulsed Film Cooling Heat Flux on a Turbine Blade Leading Edge*. ASME 2008 International Mechanical Engineering Congress and Exposition. Paper № IMECE 2008-67276, p. 1139–1149. DOI: 10.1115/IMECE2008-67276. Published Online: August 26, 2009.

[7] C.M. Bell, P.M. Ligrani, W.A. Hull, C.M. Norton. Intern. J. Heat Mass Transfer, **42**, 4333 (1999).

[8] P.M. Ligrani, C.M. Bell. Intern. J. Heat Mass Transfer, **44**, 2005 (2001).

[9] J.L. Steger. AIAA J., **16** (7), 679 (1978).

[10] K. Fletcher. *Vychislitel'nye metody v dinamike zhidkostey* (Mir, M., 1991), t. 2. (in Russian)

[11] V.M. Kovenya, G.A. Tarnavsky, S.G. Cherny. *Primenenie metoda raschepleniya v zadachakh aerodinamiki* (Nauka SO, Novosibirsk, 1990) (in Russian)

[12] S.N. Yakovenko. Teplofizika i aeromekhanika, **26**, (5), 761 (2019) (in Russian).
[13] V.V. Lemanov, V.I. Terekhov, K.A. Sharov, A.A. Shumeyko. Pisma v ZhTF,**39** (9), 34 (2013) (in Russian).
[14] P.R. Spalart, S.R. Allmaras. La Recherche Aérospatiale, **1**, 5 (1994).
[15] R.S. Solomatin, I.V. Semenov, I.S. Menshov. *K raschetu turbulentnykh techeniy na osnove modeli Spalarta–Allmarasa s primeneniem LU-SGS-GMRES algoritma* (Preprinty Keldysh IPM, 2016) № 119, 30 s. DOI: 10.20948/prepr.-2018-119 (in Russian)
[16] V.R. Efremov, V.V. Kurulin, A.S. Kozelkov, A.A. Kurkin, D.A. Utkin. hurn. vychislitel'noy matematiki i matematicheskoy fiziki, **59** (6), 1037 (2019). (in Russian)
[17] D.B. Spalding. J. Appl. Mech., **28** (3), 455 (1961).
[18] G.A. Mukhachev, V.K. Shchukin. *Termodinamika i teploperedacha* (Vysshaya shkola, M., 1991) (in Russian)

Translated by I.Mazurov